Biophysical Journal Volume 95 August 2008 1877–1889

PrP(106-126) Does Not Interact with Membranes under Physiological Conditions

Sónia Troeira Henriques,* Leonard Keith Pattenden,† Marie-Isabel Aguilar,† and Miguel A. R. B. Castanho*
*Instituto de Medicina Molecular, Faculdade de Medicina da Universidade de Lisboa, Lisbon, Portugal; and †Department of Biochemistry and Molecular Biology, Monash University, Victoria, Australia

ABSTRACT Transmissible spongiform encephalopathies are neurodegenerative diseases characterized by the accumulation of an abnormal isoform of the prion protein PrP^{Sc}. Its fragment 106-126 has been reported to maintain most of the pathological features of PrP^{Sc}, and a role in neurodegeneration has been proposed based on the modulation of membrane properties and channel formation. The ability of PrP^{Sc} to modulate membranes and/or form channels in membranes has not been clearly demonstrated; however, if these processes are important, peptide-membrane interactions would be a key feature in the toxicity of PrP^{Sc}. In this work, the interaction of PrP(106-126) with model membranes comprising typical lipid identities, as well as more specialized lipids such as phosphatidylserine and GM1 ganglioside, was examined using surface plasmon resonance and fluorescence methodologies. This comprehensive study examines different parameters relevant to characterization of peptide-membrane interactions, including membrane charge, viscosity, lipid composition, pH, and ionic strength. We report that PrP(106-126) has a low affinity for lipid membranes under physiological conditions without evidence of membrane disturbances. Membrane insertion and leakage occur only under conditions in which strong electrostatic interactions operate. These results support the hypothesis that the physiological prion protein PrP^{C} mediates PrP(106-126) toxic effects in neuronal cells.

INTRODUCTION

Prion diseases, also known as transmissible spongiform encephalopathies (TSEs), are human and animal diseases characterized by progressive neuronal loss, which is often accompanied by a spongiform brain alteration and the deposition of amyloid fibrils. These diseases appear in sporadic, familial, and infectiously acquired forms, and are invariably fatal without evoking any inflammatory or immune response in the host (1). Interest in prion diseases has grown as a result of the emergence of bovine spongiform encephalopathy and the possible infection of human beings (2).

The pathology of prion diseases is initiated by posttranslational modification of a native glycoprotein, termed prion protein (PrP), that is abundantly expressed in the central nervous system of mammalian species. A pathological scrapie form, PrP^{Sc}, interacts with the physiological form, PrP^{C}, which is converted into subsequent scrapie-form molecules ($PrP^{Sc} + PrP^{C} \rightarrow 2\,PrP^{Sc}$). The mechanism of this conversion is not well understood, but it likely takes place at the cell surface or, more specifically, in raft domains, where the PrP^{C} is preferentially located because of its glycosylphosphatidylinositol (GPI) anchor (see Naslavsky et al. (3) and Pinheiro (4) and references therein).

The two PrP isoforms possess different physicochemical properties: PrP^{C} has an α-helical structure that is susceptible to enzymatic digestion, whereas PrP^{Sc} has a large β-structure component but is resistant to proteolysis. The PrP^{Sc} forms highly insoluble, β-structure aggregates within the brain and is believed to be responsible for the neurological damage that occurs in prion diseases (5). However, PrP^{Sc} aggregates are not the only cause of pathology. It has been observed that PrP^{Sc} accumulates in intracellular compartments, and other forms of PrP (i.e., transmembrane forms (6) and a cytosolic form (7)) have also been identified. This suggests that the endosomal pathway may also be involved in disease propagation, where all these forms can be involved and take part in the propagation of the disease (see Kourie (6) and Campana et al. (8) and references therein). As a consequence of the complex pathology, the time course of PrP^{Sc} accumulation is not coincident with the time course of neurodegeneration (6).

Among all of the synthetic prion-derived peptides that have been studied, the fragment spanning the human PrP region 106-126 (KTNMKHMAGAAAAGAVVGGLG) has been identified as the most highly amyloidogenic region with neurotoxic activity. It also has the capacity to readily form fibrils (9), being partially resistant to proteolysis (10). Based on these observations, it was postulated that PrP(106-126) may be a major contributor to the physicochemical and pathogenic properties of PrP^{Sc} (11) with a role in amyloid formation and in the nerve cell degeneration that occurs in prion-related encephalopathies, and therefore PrP(106-126) was proposed as a model peptide of infectious forms of PrP (10). This evidence is supported by observations that the PrP(106-126) sequence is present in all abnormal PrP isoforms accumulated in patient brains (11), and suggests that this region may possess the ability to trigger or enable a fundamental pathogenic mechanism common to different forms of prion disease (12).

The amphipathic primary structure of PrP(106-126) is characterized by two domains: the N-terminal positive and

Submitted February 14, 2008, and accepted for publication April 18, 2008.

Address reprint requests to Miguel Castanho, Tel.: 35-1-21-798-5136; Fax: 35-1-21-799-9477; E-mail: macastaho@fm.ul.pt.

Editor: Alberto Diaspro.

0006-3495/08/08/1877/13 $2.00

doi: 10.1529/biophysj.108.131458

hydrophilic domain (KTNMKHM) and the C-terminal hydrophobic (AGAAAAGAVVGGLG) domain, which suggests a propensity to interact with cell membranes (13). Previous studies of the interaction of PrP (106-126) with model membranes have shown that pH and ionic strength are critical for secondary structure and membrane interactions, and an increased affinity for membranes at acidic pH with a concomitant increase in β-sheet content has been reported. These studies thus support the hypothesis that the endosomal pathway is involved in PrP^{Sc} formation/propagation through neuronal cells, and the PrP(106-126) region may have an effect on prion disease toxicity (14,15).

Despite the plausibility of implicating PrP(106-126) in prion disease toxicity, Fioriti et al. (12) found no evidence for PrP(106-126) infection or ability for conversion of PrP^{C} to PrP^{Sc} or to any other toxic PrP species. It has therefore been suggested that PrP(106-126) is not toxic by itself, but becomes neurotoxic in the presence of the PrP^{C} form (12,16–18), and that this toxicity is the possible result of an alteration of physiological functions of PrP^{C} instead of an effect induced by the PrP(106-126) fragment per se (12). Membrane pore formation induced by PrP(106-126) may also be an explanation for PrP toxicity, as shown by electrophysiological studies (19,20). However, this hypothesis is also controversial because pore formation (21) and neurotoxicity (22) were not confirmed by other groups.

Because of controversies surrounding PrP(106-126) toxicity, and a lack of clarity regarding a physiological role for PrP(106-126), we chose to investigate the interaction of PrP(106-126) with membranes. Because biological membranes are exceedingly complex, it is often necessary to reduce the number of membrane components to enable meaningful studies. However, since peptide-membrane interactions are often governed by the physicochemical properties of the lipid bilayer, the use of simplified model membranes, such as vesicles (e.g., large unilamellar vesicles (LUVs)), instead of neuronal cells or cellular extracts is preferred. Our experiments were carried out by means of surface plasmon resonance (SPR) with supported lipid bilayers, and by fluorescence spectroscopy methodologies with LUVs. Specifically, we investigated PrP(106-126)'s affinity for membranes, including the kinetics of PrP(106-126) membrane interactions, and the effects of PrP(106-126) on membrane stability, and the possibility of PrP(106-126) pore formation. Different conditions, including membrane charge, viscosity, lipid composition, pH, and ionic strength, were studied. The interaction between PrP(106-126) and membranes appears to be significant only at low ionic strength and high anionic-phospholipid content, which are nonphysiological conditions, and no evidence was found to support pore formation in the membranes. However, our data support models of PrP(106-126) toxicity in which a loss/modification of biological PrP^{C} function occurs within neuronal cells, as opposed to PrP(106-126) peptide being toxic by itself.

MATERIALS AND METHODS

Materials

PrP(106-126) with purity higher than 95% was obtained from Genescript Corp. (Piscataway, NJ); *N*-2-hydroxyethylpiperazine-*N*′-2-ethanesulfonic acid (HEPES), sodium chloride, L-tryptophan, acrylamide, ethanol, and chloroform were obtained from Merck (Darmstadt, Germany). The lipids 1-palmitoyl-2-oleoyl-*sn*-glycero-3-phosphocholine (POPC), 1-palmitoyl-2-oleoyl-*sn*-glycero-3-(phospho-rac-(1-glycerol)) (POPG), 1-palmitoyl-2-oleoyl-*sn*-glycero-3-(phospho-rac-(1-serine)) (POPS), 1,2-dipalmitoyl-*sn*-glycero-3-phosphocholine (DPPC), 1-palmitoyl-2-oleoyl-*sn*-glycero-3-(phospho-L-serine) (POPS), 1,2dipalmitoyl-*sn*-glycero-3-phosphoethanolamine-N(7-nitro-2-1,3-benzoxadiazol-4-yl) (N-NBD-PE), and monoganglioside GM1 were obtained from Avanti Polar-Lipids (Alabaster, AL). Congo red (CR), thioflavin T (ThT), (3-[3-cholamidopropyl)-dimethylammonio]-1-propanesulfonate (CHAPS), and cholesterol (chol) were obtained from Sigma-Aldrich (St. Louis, MO); and tris-(2-cyanoethyl)phosphine (TCEP), 1-anilinonaphthalene-8-sulfonic acid (1,8-ANS), and 4-(2-[6-(dioctylamino)-2-naphthalenyl]ethenyl)-1-(3-sulfopropyl)-pyridinium (di-8-ANEPPS) were obtained from Molecular Probes (Eugene, OR).

Working conditions and apparatus

PrP(106-126) was dissolved in sterile water to a concentration of 2 mg/mL (1.05 mM) before dilution with buffer to working conditions as described below. Experiments were conducted with final peptide concentrations in the 0–50 μM range, which is a typical concentration range for the study of cytotoxic effects and peptide aggregation (12,23–25). Throughout this study, the effect of pH was evaluated by comparing cytoplasmic physiological conditions (10 mM HEPES, pH 7.4, 150 mM NaCl) with a pH 5 endosomal mimetic (20 mM sodium acetate, pH 5, 150 mM NaCl). The effect of low ionic strength was also evaluated at pH 5 (20 mM sodium acetate, 10 mM NaCl). Experiments were performed at room temperature (25°C), under conditions where 1-Palmitoyl-2-Oleoyl-*sn*-phosphatydilcholine was in the fluid phase. A Jasco V-560 UV-vis spectrophotometer was used for all UV-vis measurements. Steady-state fluorescence measurements were carried out in a Spex FluoroLog-3 (Horiba Jobin Yvon, Edison, NJ) with double excitation and emission monochromators and a 450W xenon lamp. SPR measurements were performed in a Biacore T100 (Biacore-GE Healthcare, Uppsala, Sweden) with series S L1 sensor chips. Circular dichroism (CD) measurements were performed on a Jasco J-810 spectropolarimeter equipped with a temperature control unit.

Intermolecular β-structures determined by thioflavin T and CR

The presence of β-structures was analyzed by fluorescence emission of ThT (26) and CR absorbance (27,28). Titration of 15 μM ThT with PrP(106-126) was followed by fluorescence spectra with $\lambda_{excitation} = 450$ nm. CR absorption was followed by titration of 5 μM CR with a stock solution of PrP(106-126) to give final peptide concentrations in the range of 0–50 μM.

Peptide aggregation followed by ANS fluorescence

The effect of peptide concentration on PrP(106-126) aggregation was followed by means of ANS fluorescence emission (29–31) with excitation at 369 nm; 12.8 μM ANS ($A_{369} \sim 0.1$) was used through the experiments and titrated with a stock solution of PrP(106-126) to yield a final peptide concentration in the range of 0–50 μM.

Lipid vesicles preparation for peptide-membrane studies

LUVs are good model membranes because they have a large surface curvature that forms a consistent and stable membrane mimetic for equilibrium

studies (17,18,32). With these model membranes, different properties can be modulated (e.g., lipid charge, membrane viscosity, the presence of a sterol, the effect of pH, and ionic strength). The use of different lipid mixtures also allows the influence of selected membrane features or properties on peptide association or insertion to be explored. The LUVs used in this study were prepared from lipid films using a combination of freeze-thaw fracturing and sizing by extrusion as previously described (33). Briefly, lipid solutions in chloroform were dried under a stream of N_2 and residual organic solvent was removed in vacuo (16 h). The lipid film was hydrated with the desired buffer and subjected to eight freeze-thaw cycles to produce multilamellar vesicles (MLVs). The MLVs were extruded through polycarbonate filters (two times through a 400 nm pore size filter and eight times through a 100 nm pore size filter) to obtain LUVs. For SPR measurements the vesicles were prepared by the same procedure but extruded with a 50-nm pore size (19 times) to obtain smaller vesicles. The smaller vesicles are preferred in SPR devices to reduce fouling of microfluidics and because the more strained liposomal curvature imparts greater surface-volatility, making the liposomes easier to fuse and immobilize.

Secondary structure analysis by CD spectroscopy

CD measurements were performed to determine the secondary structure of PrP(106-126) in each lipid solution. CD spectra in the absence and presence of LUVs composed of POPC/POPG (4:1) (2-mM final lipid concentration) were carried out with 100 μM PrP(106-126) (giving a peptide lipid/ratio of 1:20) in a quartz cell with an optical path of 0.1 cm at 25°C. For these particular experiments, samples were prepared in buffer containing NaF instead of NaCl to minimize absorption by the buffer, which may mask peptide spectral features. Spectra were recorded at wavelengths between 260 and 190 nm with a 0.1-nm step and 20 nm/min speed. Spectra were collected and averaged over five scans and corrected for background contribution.

Peptide affinity for lipid membranes followed by SPR

Interaction of PrP(106-126) with lipid bilayers was studied by means of SPR. Liposomes composed of different lipid molar ratios of POPC, POPC/POPG (4:1), POPC/Chol (2:1), and POPC/GM1 (9:1) were prepared as described in the preceding section for liposomal preparation. All solutions were freshly prepared and filtered (0.22 μm) before use in the SPR and the operating temperature was maintained at 25°C throughout the assays. Small liposomal vesicles (1 mM lipid concentration) were deposited onto the L1 sensor chip surfaces (2 μL/min, 2400 s contact time), consistently reaching a steady-state plateau during deposition for all lipid mixtures. A short injection ''pulse'' of 10 mM NaOH (50 μL/min, 36 s) was used to remove loosely bound small unilamellar vesicles (SUVs), with a final stabilization period of 300 s to obtain a stable baseline. The immobilization levels were similar, with slight variations observed for different lipid compositions, but were reproducible for each composition (POPC $\sim$ 5800 response units (RU), POPC/POPG $\sim$ 4600 RU, POPC/GM1 $\sim$ 5000 RU, and POPC/Chol $\sim$ 4800 RU). Liposomal depositions resulting in surface changes of $<$6000 RU are more characteristic of supported bilayer structures than intact liposomes, which are typically $>$10,000 RU (34,35).

Peptide solutions of PrP(106-126) at different concentrations (0–50 μM) were then injected over the lipid surfaces. Sensorgrams were compared at different flow rates to examine mass transfer limitations; however, no mass transfer effects were found from flow rates of 5–20 μL/min, and the higher flow rate was used for kinetic analysis. After injection (20 μL/min, 180 s), dissociation was followed for 600 s per injection cycle and the sensor chip surface was regenerated using cycles of 20 mM CHAPS (5 μL/min, 60 s), 10 mM NaOH in 20% MeOH (50μL/min, 36 s), and 10 mM NaOH (50 μL/min, 36 s), with a final stabilization period of 600 s before subsequent liposomal capture.

The affinity of PrP(106-126) for the lipid bilayer membrane was determined from analysis and curve-fitting of a series of response curves collected with different peptide concentrations. When appropriate, association and dissociation rate constants were globally fitted using BIAevaluation version 4.1. Langmuir and two-state models were used to fit and compare data. In Langmuir kinetics the interaction follows a simple bimolecular association between peptide (P) and lipid (L):

$$P + L \underset{k_a}{\overset{k_d}{\rightleftarrows}} PL,$$

where k_a is the association rate constant, and k_d is the dissociation rate constant. The corresponding differential rate equation for this reaction model is:

$$dR/dt = k_a C_A (R_{max} - R) - k_d R,$$

where R is the response (in RU) that corresponds to the concentration of the molecular complex formed, C_A is the peptide concentration, and R_{max} is the binding capacity of the surface (36).

The two-state model is a modified version of the bimolecular model and describes a two-phase reaction as follows:

$$P + L \underset{k_{d1}}{\overset{k_{a1}}{\rightleftarrows}} PL \underset{k_{d2}}{\overset{k_{a2}}{\rightleftarrows}} PL^*.$$

In this model the first step is the initial peptide interaction with the membrane and is described by k_{a1} and k_{d1}. Peptide binding is followed by reorientation and/or insertion of the peptide into the hydrophobic core (step 2, described by k_{a2} and k_{d2}) forming the final state (PL^*) of the complex (37,38). The model assumes that dissociation of PL^* must first transition through PL before the individual species $P + L$ can then separate. The corresponding differential rate equations for this reaction model are represented by

$$dR_1/dt = k_{a1} C_A (R_{max} - R_1 - R_2) - k_{d1} R_1 - k_{a2} R_1 + k_{d2} R_2$$

and

$$dR_2/dt = k_{a2} R_1 - k_{d2} R_2.$$

$R_1 + R_2$ is the total observed response. The overall affinity constant, K, is obtained by fitted parameters as follows:

$$K = (k_{a1}/k_{d1})/(1 + k_{a2}/k_{d2}).$$

For cases in which the sensorgrams could not be fit to standard kinetic models in the association phases (see Fig. 4, *A* and *B*) and extended injection times at lower flow rates did not achieve rates of PrP(106-126)-membrane formation equal to the rates at which the complex dissociates (allowing equilibrium constants to be inferred by steady-state approximations), the RU were converted to pg/mm^2 (assuming 1 RU = 1 pg/mm^2) at the assay maximum points (t = 180s) (39). This approach allows the relative affinity to be assessed and compared based on the amount of PrP(106-126) bound to the surfaces. The kinetics was measured on these sensorgrams by fitting the dissociation phases separately from t = 200–700 s.

Membrane effects induced by the presence of PrP(106-126)

The ability of PrP(106-126) to form pores was tested for different lipid mixtures with 100 μM final lipid concentration using a methodology based on NBD fluorescence quenching by Co^{2+} ions (see Henriques and Castanho (40) and references therein). To follow the permeability of the lipid membrane to Co^{2+} ions, vesicles doped with 1% of N-NBD-PE were prepared with or without 20 mM Co^{2+} inside and outside (positive control). For the positive control, lipid was hydrated with buffer containing 20 mM Co^{2+}, allowing the quencher to be accessible to NBD in both the outer and in the inner layer. This control was compared with samples in which Co^{2+} was added after vesicle preparation; in this case Co^{2+} is accessible only to the outer layer. In the case of pore formation, after peptide addition, Co^{2+} will become accessible to the NBD fluorophores in the inner layer. Different PrP(106-126) and control concentrations

(0–50 μM) were left to incubate for 30 min and Co^{2+} was added to the samples. NBD fluorescence emission spectra were followed with $\lambda_{excitation} = 460$ nm before and after PrP(106-126) addition. Data were corrected for the inner filter effect (41). For this particular assay, MLVs were used instead of LUVs. The use of MLVs enables a gradual effect to occur in cases of translocation after pore formation, and therefore allows more reliable reading of the spectroscopic signals. Several lipid mixtures were used: POPC/POPG (1:0, 19:1, 9:1, 4:1, and 1:1), POPC/Chol (2:1), and POPC/POPG/Chol (47:20:33).

Dipolar potential in the presence of PrP(106-126) and the pH gradient effect

Membrane dipolar potential is dependent on the orientation of dipoles in the membrane/water interface. Variation in the membrane dipole potential can be used to report membrane binding and insertion of molecules by recording fluorescence excitation spectra of di-8-ANEPPS-labeled vesicles, which are particularly sensitive to dipolar potential variations (42). In this part of the study, 25 μM PrP(106-126) was added to LUVs with 200 μM lipid and 4 μM dye (di-8-ANEPPS is not fluorescent in aqueous medium). To detect spectral variations in di-8-ANEPPS excitation, the spectrum ($\lambda_{emission} = 570$ nm) in the absence of the peptide was subtracted from the spectrum in the presence of 25 μM PrP(106-126) (both spectra were normalized to total integrated area). This differential spectrum enables detection of peptide-induced changes in the membrane dipolar potential (42,43). Fresh solutions and aged peptides (48 h, 37°C) were compared in these experiments. Several lipid compositions were used: POPC/POPG (1:0, 4:1, 7:3, 3:2, 1:1 and 0:1) to evaluate the charge effect; POPC/POPS (4:1) to test any particular effects with serine; POPC/Chol (1:0, 41:9, and 2:1) to evaluate the effects of the presence of cholesterol; and POPC/GM1 (1:0, 19:1, 9:1, 4:1, and 1:1) and a mixture of POPC/POPG/Chol/GM1 (37:20:33:10) to test whether a more complex lipid mixture would improve the interaction with membranes. Liposomes with a pH gradient (pH 5.0 inside and pH 7.4 outside liposomes) were prepared to mimic the environment at the endosome/cytoplasm interface. POPC/POPG (1:1) vesicles were tested. Controls with pH 7.4/pH 5 (in/out), pH 7.4 (in/out), and pH 5 (in/out) were performed.

RESULTS

Previous works have attributed several toxic properties to the Prp(106-126) fragment (9,11,24). Our aim was to elucidate the possible involvement of cellular membranes in the toxicity of PrP(106-126). LUV model membranes were used in this study because LUVs have a very large curvature at the molecular scale and can be considered planar for these purposes, and therefore LUVs are good model membranes to evaluate peptide-membrane interactions (32). Different lipidic mixtures were used to mimic different membrane properties under three different buffer conditions: 1), pH 7.4, 150 mM NaCl to evaluate the membrane-binding properties of PrP(106-126) (analogous to physiological conditions); 2), pH 5, 150 mM NaCl to evaluate the possible interaction of PrP(106-126) with endosomes where some toxic PrP species have been localized and possible PrP^{Sc} propagation has been suggested (8); and 3), pH 5 with low ionic strength (10 mM NaCl) to evaluate the possible contribution of electrostatic interactions to membrane affinity.

PrP(106-126) aggregates in aqueous solution and forms amyloid fibrils

Previous studies have shown that PrP(106-126) tends to aggregate and to form β-structures in a similar manner to the scrapie PrP isoform (9,44). To verify that the same process would occur under the conditions of this study, the formation of β-sheet aggregates was tested by the fluorescence of ThT and the absorbance of CR. These two dyes are widely used to detect the formation of amyloid structures (30).

In the absence of β-sheet aggregates, the ThT dye has an excitation and fluorescence emission maxima at 350 and 438 nm, respectively. In the presence of amyloid fibrils the ThT spectra shift to 450 nm and 482 nm, respectively (26). During titration of ThT with PrP(106-126) a slight increase in the fluorescence intensity at 482 nm, characteristic of ThT interacting with β-sheet structures, was observed (data not shown). Although this effect was not strong, it was not unexpected, since even some β-sheet-rich proteins are reportedly unable to induce the characteristic ThT fluorescence (45).

CR absorbance was used to determine whether this peptide adopts a significant β-sheet conformation. In the case of amyloid fibril formation, a red shift in the CR absorbance spectrum at physiological pH is expected (27,28). At pH 7.4, 150 mM NaCl the CR maximum appears at 489 nm. When CR was titrated with PrP(106-126), a gradual red shift in absorbance spectra was observed (Fig. 1 *A*) as a result of an increase in the component at 535 nm (see differential spectra *inset* in Fig. 1 *A*). At pH 5, 150 mM NaCl, the CR absorbance spectrum peaks at 502 nm, which is blue-shifted in the presence of PrP(106-126) (Fig. 1 *B*). An increase at 496 nm was detected in the differential spectra (see inset in Fig. 1 *B*). At pH 5 the histidine residue is protonated, which increases the electrostatic effects and the affinity of CR for the peptide, in agreement with observations for other amyloid peptides (46). Binding of CR to the peptide leads to a dramatic change on the spectral shift even in the first peptide addition (2 μM). Since the spectral shifts stabilize at 1:1 stoichiometry (47), peptide-peptide interactions at excess peptide (i.e., greater than 5 μM) do not further shift the spectrum because all of the CR is already bound. However, conformational alterations of the peptide still occur and lead to alterations in the conformational dynamics of CR, resulting in changes in intensity even after spectral shifts have reached a maximum (see Fig. 1 *B*).

Though the direct comparison of the effects on CR absorbance at pH 5 and pH 7.4 is not straightforward because CR absorbance properties change with pH (15,47), we conclude that at pH 7.4 and pH 5, PrP(106-126) is able to interact with CR as an indicator of β-sheet conformation (46).

As a further test, the possibility of peptide aggregation was also followed by means of ANS fluorescence. The ANS dye is sensitive to the polarity of its microenvironment and is frequently used to identify the presence of hydrophobic ''pockets'' in proteins and peptides (29–31). In the presence of hydrophobic ''pockets'', ANS fluorescence emission intensity increases and concomitantly undergoes a blue shift.

Titration of ANS with PrP(106-126) at pH 7.4 (150 mM NaCl) causes an increase in the fluorescence intensity and a

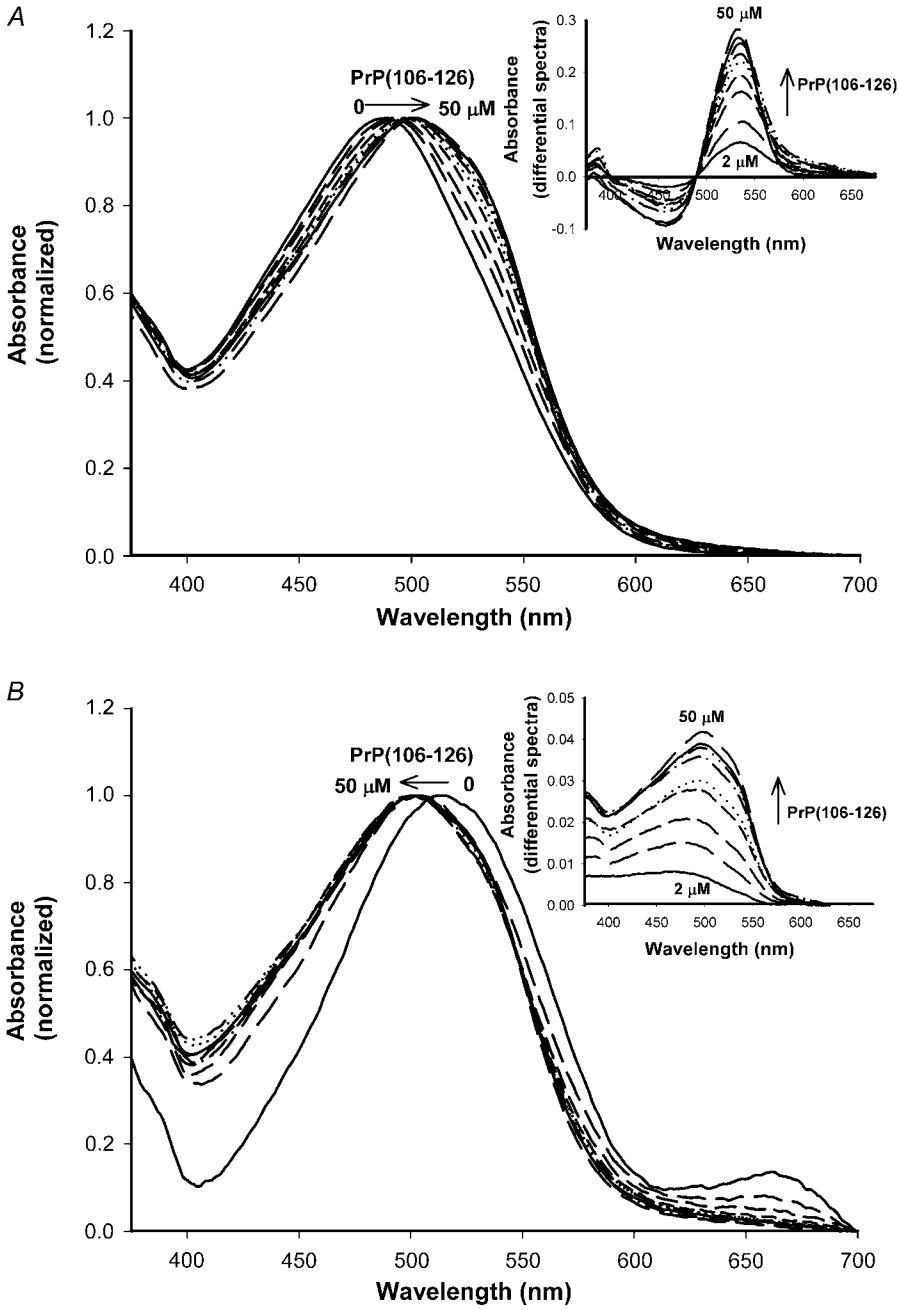

FIGURE 1 Identification of β-structures in the PrP(106-126) by CR absorbance. Absorbance spectra of 5 μM CR in the presence of PrP(106-126) 0–50 μM (*A*) at pH 7.4, 150 mM NaCl, and (*B*) at pH 5, 150 mM NaCl. Absorbance was normalized to highlight the red shift at pH 7.4 and the blue shift at pH 5.0 upon peptide addition. (*Inset*) Initial CR absorbance spectrum was subtracted to all the spectra obtained after peptide addition at pH 7.4 or pH 5. At pH 7.4 an increase is seen in the CR absorbance at 535 nm with peptide concentration, and at pH 5 there is an increase at 496 nm. This indicates that PrP(106-126) is interacting with CR, which suggests that PrP(106-126) has a β-structure. This effect is stronger at pH 7.4 compared to pH 5.

significant blue shift (59 nm) of the maxima of ANS emission (Fig. 2), which is indicative of the presence of aggregates in solution. This same shift was also detected at pH 5 and for both for low and physiological ionic strengths (data not shown).

CD spectroscopic analysis of PrP(106-126) secondary structure

The results of the experiments with ThT and CR dyes, and previous publications (14) on PrP(106-126) secondary structure, suggest the presence of β-sheet secondary structure in solution. CD was therefore used to study the secondary structure of the peptide upon interaction with the model membranes. Fig. 3 shows the CD spectra of 100 μM PrP(106-126) in the presence and absence of POPC/POPG (4:1) LUVs ([Lipid] = 2 mM), with no α-helix signal found under any conditions (double minima bands at 208 and 222 nm, and a positive band at 192 nm). Under acidic conditions the CD spectra have a predominantly random coil structure (as characterized by the well-defined strong negative minima at ~195 nm). Upon interaction with membranes, there is a shift to 204 nm and a concomitant decrease in intensity, without gains in characteristic α-helix components, indicating that an extended conformation is predominant in the

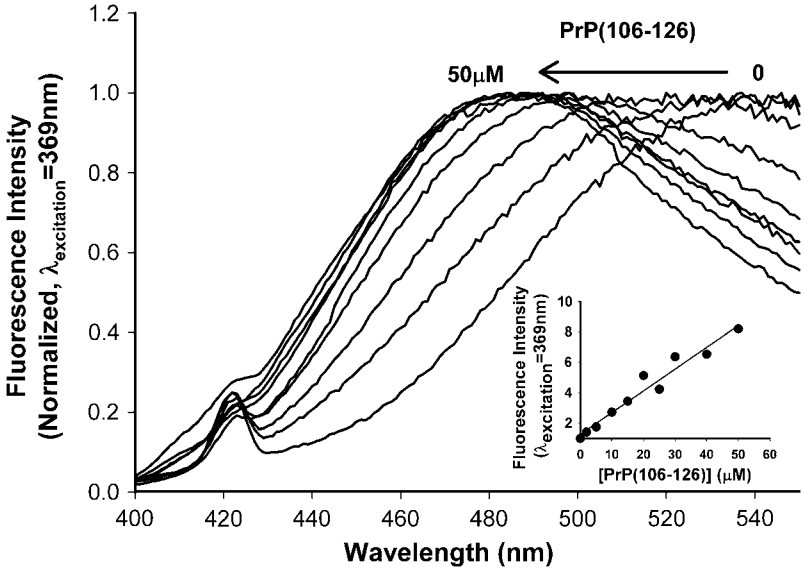

FIGURE 2 Aggregation of PrP(106-126) evaluated by ANS fluorescence properties. The effect of peptide concentration in 12.5 μM ANS fluorescence emission spectrum ($\lambda_{excitation} = 369$ nm, pH 7.4, 150 mM NaCl). Spectra were normalized to highlight the ANS blue shift upon interaction with PrP(106-126). (*Inset*) Dependence of integrated fluorescence intensity of ANS with peptide concentration. A significant blue shift and a concomitant increase in ANS fluorescence intensity indicate that this peptide is in an aggregated form.

presence of membranes. Under physiological conditions there was no alteration in the minima position in the presence of liposomes. Overall, the results demonstrate that PrP(106-126) has no discernible helicity and very little secondary structure in the presence or absence of the POPC/POPG membranes at different pHs.

PrP(106-126) interaction with membranes—kinetics and affinity

The interaction and affinity of PrP(106-126) for lipid bilayers was studied by means of SPR with lipid membranes adsorbed onto an L1 sensor chip, which contains a dextran matrix with substituted lipophilic alkyl chains that give the surface lipophilic properties. SPR has proven to be a valuable experimental approach to study the interaction of peptides with lipid bilayers, which allows the real-time monitoring of peptide binding to and dissociation from lipid bilayers, and has the advantage of obviating the need to use labeled peptides or lipids (38). Liposomes are captured on the surface of the sensor chip and the peptide is passed across the formed membrane. SPR detects changes in the refractive index at a maximal depth of 300 nm in the flow cell, providing real-time measures of association/dissociation of the peptide at the membrane sensor surface. The surface RU is proportional to the adsorbed mass on the sensor surface (38).

In this study we examined the association/dissociation of PrP(106-126) with membranes using different lipid compositions to gain more insight into the parameters that govern the membrane affinity and selectivity of the peptide. Model membranes of POPC were compared with membranes with more complex lipid compositions, such as POPC/POPG (4:1), POPC/Chol (2:1), and POPC/GM1 (9:1).

Phospholipids with a phosphatidylcholine (PC) headgroup are the major component in mammalian cell membranes (48). POPC vesicles at room temperature are in fluid phase and can be used to represent the bulk phase in cell membranes. Negatively charged phospholipids are more abundant in the inner leaflet of the plasma membrane (48) and have been implicated in amyloid fibril stimulation in vivo (49). The potential role of negatively charged lipids in the membrane binding of PrP(106-126) was therefore evaluated through the use of membranes composed of POPC/POPG. This binary mixture maintains fluid phase properties.

Because neuronal cell membranes are enriched with cholesterol, and a specific involvement of cholesterol has been implicated in PrP^{C}-PrP^{Sc} conversion in prion-infected cell lines from cholesterol-depletion studies (50,51), the possible interaction of PrP(106-126) with cholesterol was also tested with vesicles composed of POPC/Chol (2:1), which presents a homogeneous liquid-ordered phase (52). Therefore, the effect of membrane rigidity on peptide-membrane interaction can be studied and compared with membranes on fluid phase. Finally, GM1 is a ganglioside that is abundantly expressed in neurons and concentrated in caveolae and lipid raft regions, and has been shown to bind specifically to the Alzheimer's Aβ peptide leading to the induction of β-structure (53–55) and possibly membrane disruption (56). The similarities in the amyloidogenic properties of the Aβ peptide and PrP in prion disease raises the question as to whether GM1 may also induce β-structure in PrP(106-126), and whether GM1 may be involved in the membrane affinity of PrP(106-126). This possibility was explored in this study using vesicles composed of POPC/GM1(9:1). At this lipid ratio, GM1 has been reported to form rigid microdomains in the PC bilayer (57,58).

The effect of pH and ionic strength on the interaction of PrP(106-126) with POPC is shown in Fig. 4 *A*, and the influence of lipid composition at low pH and ionic strength is shown in Fig. 4 *B*. The sensorgrams indicate that under

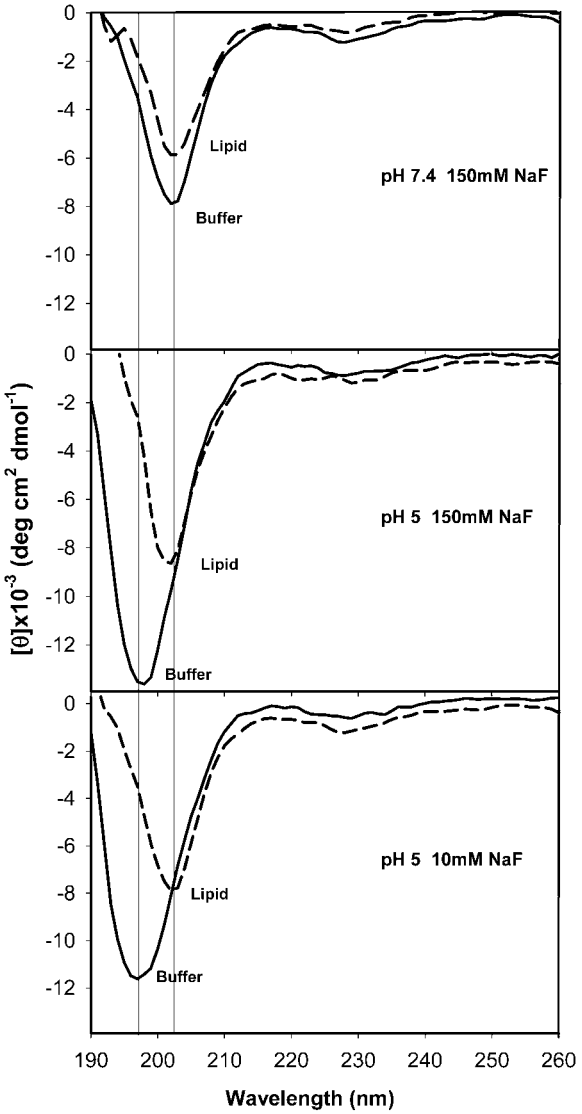

FIGURE 3 CD spectra of 100 μM PrP(106-126) in the presence and absence of POPC/POPG (4:1) LUVs ([Lipid] = 2 mM). Three conditions were tested: 10 mM HEPES buffer, pH 7.4, 150 mM NaF; 20 mM acetate buffer, pH 5, 150 mM NaF; and 20 mM acetate buffer, pH 5, 10 mM NaF. No α-helix (double minima bands at 208 and 222 nm and a positive band at 192 nm) is observed for PrP(106-126) under any conditions. At pH 5 (but not pH 7.4), the CD spectra have a strong negative band at 198 nm (random coil structure), with a shift upon interaction with membranes to 204 nm. Both minima in the presence and absence of membranes remain at the same wavelength for pH 7.4 conditions (204 nm).

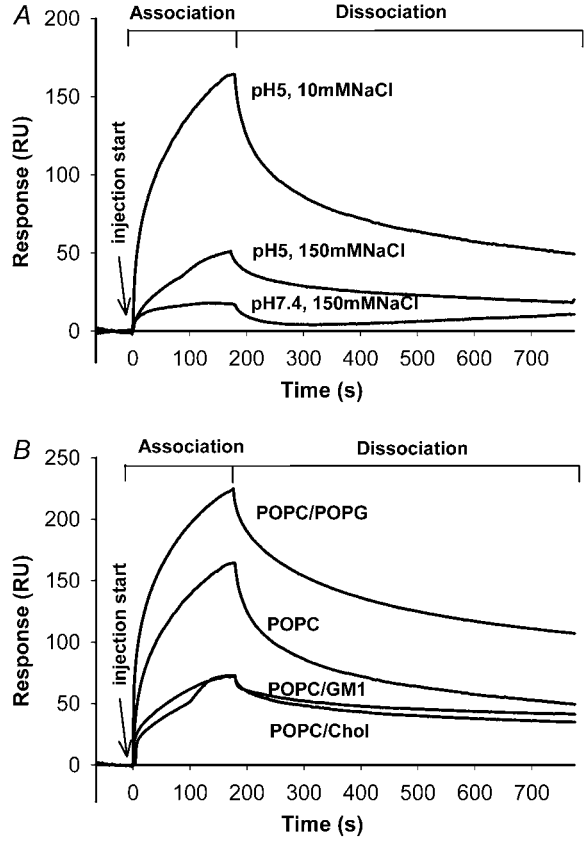

FIGURE 4 Influence of lipid and buffer composition on peptide affinity for membranes. (*A*) pH and ionic strength effect on PrP(106-126) (25 μM) interaction with POPC membranes immobilized on the surface of an L1 chip. HEPES buffer pH 7.4, 150 mM NaCl; acetate buffer pH 5, 150 mM NaCl; and acetate buffer pH 5, 10 mM NaCl were used. The peptide does not show a significant affinity for membranes under physiological conditions. At acidic pH a marked increase in the membrane-bound peptide is observed, which is significantly enhanced at low ionic strength. (*B*) The affinity of 25 μM PrP(106-126) for membrane surfaces on L1 chips is shown for different lipidic compositions at pH 5, 10 mM NaCl. Compositions are: POPC, POPC/POPG (4:1), POPC/Chol (2:1), and POPC/GM1 (9:1). PrP(106-126) has a lower binding to POPC/Chol and POPC/GM1 relative to POPC and the highest affinity for the anionic membrane.

physiological conditions (pH 7.4, 150 mM NaCl) the peptide does not bind as strongly to POPC membranes, with only 17.3 pg/mm^2 PrP(106-126), bound at $t = 180$ s (see Fig. 4 *A*). Whereas a slightly better interaction is evident for POPC at pH 5, 150 mM NaCl (47.1 pg/mm^2), a significant increase in the RU signal is observed at pH 5 and low ionic strength (164 pg/mm^2).

A comparison of the POPC membrane binding and POPC/POPG (4:1) reveals a significant charge effect with an increase in the amount of peptide bound in the presence of the anionic phospolipid (Fig. 4 *B*, Table 1). In contrast, the interaction of PrP(106-126) with POPC/Chol (2:1) and POPC/GM1 (9:1) was weaker than that with POPC under all buffer conditions tested (Fig. 4 *B*, Table 1). However, it is noteworthy that although there was less material bound to the cholesterol and GM1 membranes, there was also a slower dissociation from the membrane in the presence of cholesterol and GM1 (Table 1).

A kinetic analysis of concentrations of PrP(106-126) up to 25 μM with POPC and POPC/POPG(4:1) at pH 5, 10 mM NaCl, conditions (Fig. 5) shows that PrP(106-126) has a higher affinity for the POPC/POPG membranes at pH 5 (low ionic strength). The PrP(106-126) interaction with these membranes follows a two-state binding model, which assumes that a change occurs in the structure and/or orientation

TABLE 1 The amount of PrP(106-126) bound to and dissociation rate (k_d) from POPC, POPC/POPG (4:1), POPC/Chol (2:1), and POPC/GM1 (9:1) membranes assayed in acetate buffer, pH 5 (10 mM NaCl)

Lipid type	Peptide bound (pg/mm^2)	k_d ($\times 10^{-3}$ 1/s)
POPC	164	1.1
POPC/POPG (4:1)	225	0.77
POPC/Chol (2:1)	72.7	0.46
POPC/GM1 (9:1)	48.5	0.67

Amount of peptide bound to membranes was calculated after 25 μM injection at the assay maxima points ($t = 180$ s) (assuming 1 RU = 1 pg/mm^2; see Fig. 4 *B*). Dissociation constants were obtained after dissociation curve-fitting using BIAevaluation version 4.1.

of the peptide after initial binding to the membrane. The two-state binding model resulted in a significant improvement in fit quality compared to the 1:1 Langmuir model (the two-state kinetic and affinity constants are presented in Table 2). In this model the values k_{a1}/k_{d1} characterize the first step or ''encounter complex'', whereas k_{a2}/k_{d2} describe peptide reorientation and/or insertion of the peptide into the hydrophobic core. The importance of electrostatic forces on PrP(106-126) membrane binding is evidenced by larger association rates ($k_{a1} = 5.04 \times 10^2$ 1/Ms, $k_{a2} = 5.3 \times 10^{-3}$ 1/s for POPC, and $k_{a1} = 21.4 \times 10^2$ 1/Ms, $k_{a2} = 13.7 \times 10^{-3}$ 1/s for POPC/POPG 4:1) and larger overall affinity constants ($K = 1.26 \times 10^5$ 1/M, and 4.39×10^5 1/M for POPC and POPC/POPG (4:1), respectively) in the presence of negatively charged phospholipids.

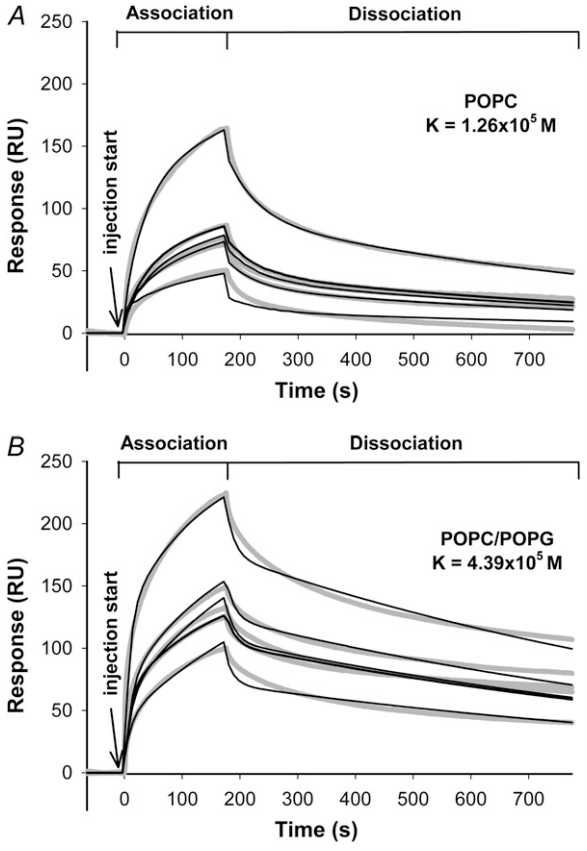

FIGURE 5 Global two-state kinetic analysis of SPR data PrP(106-126) in the presence of (*A*) POPC or (*B*) POPC/POPG (4:1) membranes captured on L1 chip surfaces. Peptide samples (5, 10, 15, 20, and 25 μM) were prepared in acetate buffer (pH 5, 10 mM NaCl) and injected at 20 μL/min flow rate. Sensorgrams were corrected for bulk shift effect (*shaded lines*) and a two-step binding model was fitted to data with BIAevaluation version 4.1 (*solid lines*). Kinetic and affinity constants are presented in Table 2.

PrP(106-126) does not form ionic channels under physiological conditions

One possible mechanism by which PrP(106-126) exerts toxic effects is via channel formation across cell membranes. To determine whether pore formation occurs, we took advantage of the ability of Co^{2+} to quench NBD fluorophores (for further details see the Materials and Methods section). SPR results demonstrated that PrP(106-126) binds preferentially to vesicles with negatively charged phospholipids. The results in Fig. 6 show that PrP(106-126) was not able to make vesicles permeable to Co^{2+} ions, regardless of the molar ratio of POPG tested at physiological conditions. At acidic pH, significant quenching was only apparent at low ionic strength (10 mM NaCl) and a high POPG molar ratio (1:1; Fig. 6). These results demonstrate that Co^{2+} permeability can only be achieved when electrostatic interactions are dominant between PrP(106-126) and negatively charged vesicles. Serine-containing glycerophospholipids are the most common negatively charged phospholipids present in mammalian cells. To evaluate whether there is any particular effect with serine, POPC/POPS was also tested and no difference was observed in the capacity to induce channel formation (results not shown). The presence of cholesterol and GM1 was also tested by the use of liposomes composed of POPC/Chol (2:1) and POPC/GM1 (9:1), but no leakage was observed in these liposomes or in the more-complex lipid mixtures of POPC/POPG/Chol (47:20:33) in any of the buffer conditions tested.

Effect of PrP(106-126) on membrane potential and the pH gradient

Peptide insertion into lipid bilayers will perturb the membrane dipolar potential, which can be monitored by means of a spectral shift in the excitation spectra of di-8-ANEPPS (43). This dye is located in the lipid headgroup region, where it is sensitive to the local electric field (42). To screen the interaction of PrP(106-126) with membranes, a fresh or aged solution of 25 μM PrP(106-126) was added to liposomes with different lipid compositions: POPC/POPG (1:0, 4:1, 7:3, 3:2, 1:1, and 0:1), POPC/POPS (4:1), POPC/Chol (1:0, 41:9 and 2:1), POPC/GM1 (1:0, 19:1, 9:1, 4:1, and 1:1), and a mixture of POPC/POPG/Chol/GM1 (37:20:33:10). A noticeable spectral shift in di-8-ANEPPS was only observed at

TABLE 2 Association (k_{a1} and k_{a2}), dissociation (k_{d1} and k_{d2}), and affinity constant (K) of PrP(106-126) binding to POPC and POPC/POPG (4:1) assayed in acetate buffer, pH 5 (10 mM NaCl)

Lipid type	k_{a1} ($\times 10^2$ 1/Ms)	k_{d1} ($\times 10^{-2}$ 1/s)	k_{a2} ($\times 10^{-3}$ 1/s)	k_{d2} ($\times 10^{-3}$ 1/s)	K ($\times 10^5$ M^{-1})	χ^2
POPC	5.05	1.35	5.30	1.56	1.26	5.14
POPC/POPG (4:1)	21.4	5.69	13.7	1.17	4.39	13.9

Binding constants were obtained after fitting the SPR data from Fig. 5 to a two-state binding model with BIAevaluation version 4.1. Experimental conditions are described in the legend of Fig. 5.

pH 5 (10 mM NaCl) in lipid vesicles composed of POPC/POPG (1:1) (Fig. 7).

Because a pH gradient can promote the translocation of some peptides across a membrane (59), we also investigated whether a pH gradient across the endosomes/cytoplasm can promote PrP(106-126) interaction with membranes and subsequently induce membrane translocation. With a constant ionic strength (150 mM NaCl), a pH gradient across membranes was created in POPC/POPG (1:1). Liposomes with pH 5/pH 7.4 (in/out) were compared with pH 7.4/pH 5 (in/out), pH 7.4 (in/out), and pH 5 (in/out) 150 mM NaCl. No significant differences were detected between the samples with a pH gradient and the controls (see Fig. 7).

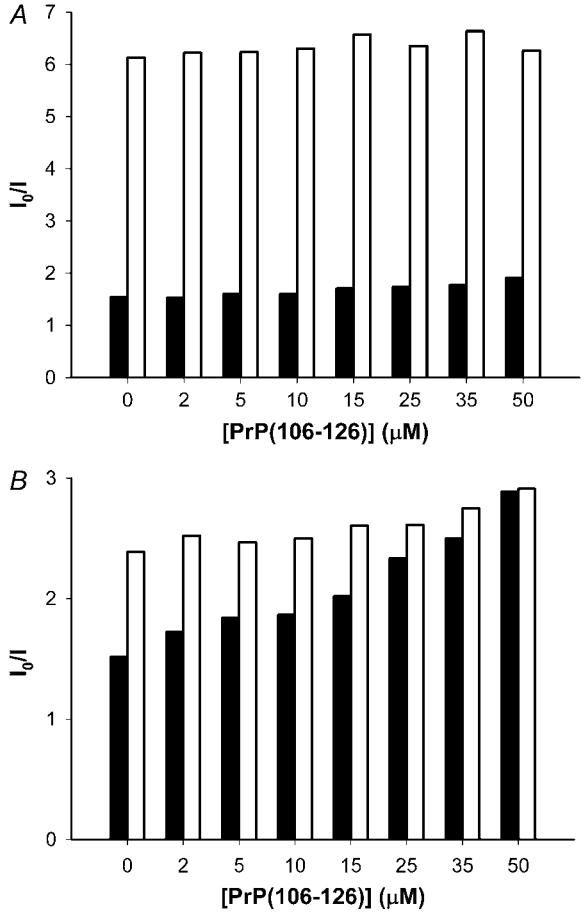

FIGURE 6 Cross-bilayer channel formation induced by PrP(106-126) in 100 μM POPC/POPG (1:1) vesicles followed by NBD quenching by Co^{2+}. The ratio of NBD fluorescence emission ($\lambda_{excitation} = 460$ nm) in the absence of quencher (I_0) and the presence of 20 mM Co^{2+} (I), for the vesicles with Co^{2+} accessible to both layers (*open columns*) and for the vesicles where Co^{2+} is only accessible to the outer layer (*solid columns*), is presented for different peptide concentrations. These experiments were carried at pH 5 (*A*) 150 mM NaCl or (*B*) 10 mM NaCl. A comparison of the results (*solid columns*) with the positive control (*open columns*) demonstrates that pores are not formed, even at a high peptide/lipid ratio (1:2, for 50 μM PrP(106-126)), at 150 mM NaCl. At 10 mM NaCl there is increased leakage of Co^{2+} with increasing peptide concentration.

DISCUSSION

Prion disease is initiated by conversion of physiological PrP^C, a protein abundantly expressed in mammalian brain, into a pathological isoform, PrP^{Sc}, which accumulates within the brain as highly toxic insoluble aggregates (1). The neurodegeneration rate verified in prion disease cannot be explained solely by PrP^{Sc} formation and deposition (6). Some other PrP toxic species have been identified inside the cells, which seem to have an important role in disease propagation and transmission after infection by PrP^{Sc} (6). A neurotoxic PrP fragment, PrP(106-126), that has physicochemical properties similar to PrP^{Sc} and is present in all abnormal toxic

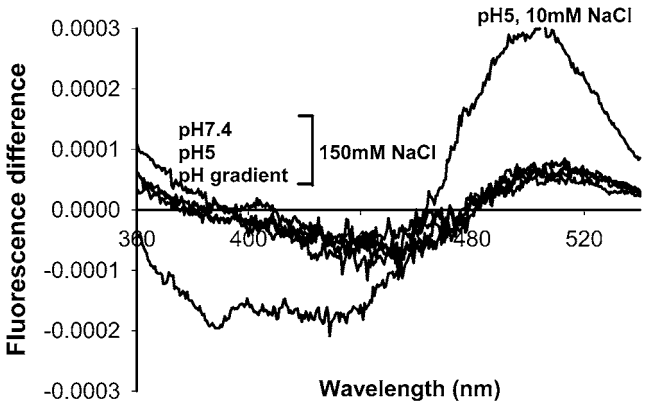

FIGURE 7 PrP(106-126) effect in the dipolar potential of POPC/POPG (1:1) vesicles followed by fluorescence difference spectra of Di-8-ANEPPS-labeled vesicles. The excitation spectrum obtained in the absence of peptide was subtracted to the spectrum obtained in the presence of 25 μM PrP(106-126); both spectra were normalized to the integrated areas to reflect only the spectral shift. The difference spectrum obtained in acetate buffer, pH 5 (10 mM NaCl), has a more pronounced shift than the other four difference spectra obtained with 150 mM NaCl (pH 7.4, pH 5) or with a pH gradient pH 7.4/pH 5 (in/out) and pH 5/pH 7.4 (in/out). PrP(106-126)'s effect on the dipolar potential is therefore independent of pH or pH gradient, but depends on ionic strength.

species within the patient brain has been used as a model of PrP^{Sc} to study the possible mechanism of disease propagation and transmission (9–12,14,44). However, PrP(106-126) toxicity remains controversial in the literature. Nonselective pore formation leading to ionic gradient destabilization has been proposed as a mechanism by which PrP(106-126) exerts its neurotoxic effects (19); however, channel formation was not reproduced in some reports (21) and the neurotoxicity of this peptide was verified only in the presence of PrP^{C} (17,18).

The aim of this work was to determine whether PrP(106-126) interacts with model membranes, and whether this interaction correlates with the biological toxic effects of PrP(106-126). PrP(106-126) was characterized in the absence/presence of liposomes under three different buffer conditions. Whereas PrP(106-126) formed aggregates in the buffer solutions used (Fig. 2), no significant secondary structure was apparent in the presence of liposomes (Fig. 5).

The interaction of PrP(106-126) with lipid membranes was evaluated by SPR and correlated with fluorescence methodologies that report on variations in the dipolar potential at the membrane. Under physiological conditions of pH 7.4 and 150 mM NaCl, PrP(106-126) interacted relatively weakly with all lipid mixtures used. A lower affinity for membranes at physiological buffer conditions was confirmed by membrane dipolar potential studies and leakage measurements. Moreover, neither PrP(106-126) insertion nor membrane leakage was observed under any of these conditions.

At pH 5, the histidine residue at position 6 in the PrP(106-126) sequence is ionized and the formal net charge of the peptide increases from +2 (contributed from the two lysine residues) to +3 (6). With pH 5, 150 mM NaCl, a slight increase in membrane affinity was detected by SPR on POPC membranes (Fig. 4 *A*). This affinity was greatly increased with low ionic strength (10 mM NaCl) (Fig. 4 *A*, topmost sensorgram) and in the presence of POPG (a negatively charged phospholipid) (Fig. 4 *B*). Under these conditions, electrostatic interactions between the positively charged peptide and negatively charged membrane are enhanced, which increases the overall peptide-membrane affinity (see Table 2); however, no insertion or pore formation was detected as verified by monitoring membrane dipolar variation and by leakage experiments.

It has been suggested that amyloid formation is stimulated in the presence of a hydrophobic environment at acidic pH (60). Our results show no significant secondary structure in the presence or absence of lipid under different buffer conditions (see Fig. 5). SPR shows that the interaction of PrP(106-126) with membranes at pH 5 10 mM NaCl can be described by a two-state model. The two states may be identified as: step 1), peptide interaction with the membrane interface (primarily governed by electrostatic interactions between the peptide and the membrane); and step 2), the peptide undergoes a secondary structure modification at the bilayer surface/or lipidic rearrangements occur in the membrane, resulting in a complex that cannot dissociate from the surface without first transitioning back through the kinetic pathway. This second step involves underlying thermodynamic events, including a transition of the peptide into the plane of binding, which depends on the hydrophobic/hydrophilic balance of the molecules groups and forces involved (61) and can be dependent on the interfacial hydrophobicity of the peptide (62). For PrP(106-126), a White-Wimley hydrophobicity prediction (see Fig. 8) does not favor interfacial partitioning irrespective of the peptide charge state, and so an increase in partitioning at low ionic strength results from the increase in peptide concentration close to membrane environment and is dependent on the electrostatic interactions of the membrane and peptide. Furthermore, because no insertion or dipole changes were detected with the membrane under any of the fluorescent experiments to support an insertion hypothesis, we conclude that the second step in the two-state interaction can only be subtle peptide-membrane changes local to the membrane surface.

The SPR experiments also indicated that PrP(106-126) does not bind specifically to ganglioside GM1 or cholesterol. GM1 has a tendency to form microdomains in PC membranes (57,58) and is known to bind the Alzheimer's Aβ peptide, leading to the induction of β-structure (53–55) and possibly membrane disruption (56). However, the SPR and fluorescence data indicate that clustering of GM1 in more organized patterns may actually hinder the interaction of PrP(106-126) with POPC due to steric constraints of the sugar headgroups leading to an apparent lower affinity for POPC/GM1 than for POPC at acidic pH (Fig. 3 *B*). However, the k_d values suggest that although lower amounts of peptide bound to the GM1 surface, once the peptide interacts with the surface it remains bound for a longer period of time.

Some observers have suggested that cholesterol may play a role in decreasing PrP^{C}-PrP^{Sc} conversion (50,51); therefore, cholesterol was specifically included in this study. POPC/Chol (2:1) vesicles have a homogeneous liquid-ordered phase. However, the combined evidence of reduced affinity

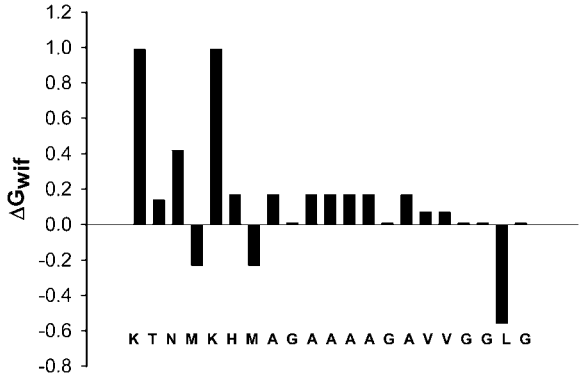

FIGURE 8 Theoretical analysis of PrP(106-126) partition into interfacial membrane region-based free-energy change ΔG_{wif} from water transfer to the lipid membrane interface (see White and Wimley (62)). Residues with values $\Delta G_{wif} < 0$ have a tendency to be transferred from the water phase to the membrane.

observed by SPR, lack of fluorescence evidence for membrane changes, and lack of peptide insertion or leakages leads us to conclude that PrP(106-126) does not bind specifically to cholesterol in the plasma membrane and does not have a preference for the liquid-ordered phase.

Membrane insertion and channel formation, as determined from Co^{2+} leakage and variation of the membrane dipolar potential, were detected only with model membranes composed of POPC/POPG (1:1) at pH 5, 10 mM NaCl. Under these extreme conditions the membrane has a strong negative charge and the low ionic strength is not sufficient to prevent a strong electrostatic attraction to the positively charged peptide. The possible importance of endosomes in PrP propagation was evaluated by mimicking the pH gradient in the cytoplasm/endosome environment. The pH gradient (pH 7.4/5 (in/out) or pH 5/7.4 (in/out)) could eventually be a driving force for peptide insertion in the membrane, as observed for other peptides (59). However, both pH gradient systems failed to show any evidence that PrP(106-126) inserts into the membrane (see Fig. 7).

Altogether, these peptide-membrane studies show that PrP (106-126) does not have a strong affinity for lipid membranes under conditions similar to the cytoplasmic environment. Under conditions that mimic the endosomal environment, PrP(106-126) also has a weak interaction with membranes, and in these conditions no insertion or pore formation were detected.

These observations indicate that the toxic effects of PrP(106-126) cannot be explained by cell membrane leakage. Alternatively, it can be hypothesized that the PrP(106-126) toxic effects occur inside the cell. Such suggestions imply PrP(106-126) cellular internalization, which is a phenomenon that has been demonstrated for several peptides, such as the cell-penetrating peptides (CPPs) family (63). The uptake of CPPs can follow two routes: one is physically mediated and the other is dependent on the endosomal pathway. Both routes require peptide-membrane interactions as the first step (64). With the lack of affinity of PrP(106-126) for lipid membranes, both routes for cell entry can be discounted, unless the cellular internalization of PrP(106-126) occurs via a mechanism mediated by the presence of physiological PrP (e.g., mediated by caveolae or rafts where PrP is colocalized on the cell surface). The N-terminal domain of PrP with a noncleaved signal sequence has been included in the CPP family because of its ability to translocate across cell membranes (65). This sequence may be responsible for the internalization of sizeable cargo into cells (65). It has been suggested that this N-terminal domain is implicated in PrP trafficking as well as in prion infectivity (65). A possible internalization of PrP(106-126) in cells mediated by this N-terminal domain of PrP could explain the possible toxic effects inside cells after internalization.

In the work presented here, we tested whether PrP(106-126) has affinity for the membrane in an endosomal-like environment. An increased propensity to interact with lipid bilayers (see Fig. 3 *A*) was evident; however, this does not represent a significant membrane insertion (see Fig. 7) or an improved tendency to form a transmembrane pore. This is in agreement with previous findings that the fibrillogenic properties alone are not sufficient for neurotoxicity, as verified by other PrP fragments that were able to assemble into filaments but lacked toxic effects (9). Moreover, even with a pH gradient across the membrane, similar to the endosomal/cytoplasmic interface, no insertion in the membrane was observed. Therefore, in the case of the PrP(106-126) fragment endosomal internalization, the toxic effect cannot be explained by acidic pH. Altogether, our data lead us to conclude that pore formation or any direct effect on membrane properties does not occur and hence is not involved in PrP(106-126) toxicity.

Our results corroborate previous reports in which pore formation was not detected in the presence of PrP(106-126) (21). Studies performed with the complete PrP molecule have also proposed membrane leakage as a possible mechanism for toxicity (66,67). In these studies, membrane leakage was performed with SUVs composed of POPG and in the absence of salt (66,67). Liposomes with such characteristics are unstable not only because of the high membrane curvature (32) but also because of charge repulsion in the absence of counter ions. Moreover, leakage of zwitterionic membranes composed of POPC or DPPC/Chol/sphingomylin was not significant (67). When these observations are combined with the results of the study presented here, it is possible to conclude that PrP(106-126) disturbs the lipidic bilayers only in extreme conditions. This in turn adds weight to the hypothesis that PrP^C may be necessary to mediate PrP(106-126) toxicity (12). One possible mechanism is that the peptide kills neurons by modification/inhibition of a physiological function of PrP^C. In such a scenario, PrP(106-126) toxicity would be related to a loss of PrP function rather than a gain of toxic properties in the presence of PrP(106-126) (12).

We thank Dr. Andrew Miles (Birkbeck College, London) for comments regarding circular dichroism during the preparation of this manuscript.

This work was supported by a grant from Fundação para a Ciência e Tecnologia (SFRH/BD/14337/2003 to S.T.H.). The International Union of Biochemistry and Molecular Biology is acknowledged for financial support to S.T.H. for a short-term visit to the Marie-Isabel Aguilar laboratory at Monash University, Victoria, Australia. The support of the Australian Research Council and the Potter Foundation is gratefully acknowledged.

REFERENCES

1. Prusiner, S. B. 1998. Prions. *Proc. Natl. Acad. Sci. USA*. 95:13363–13383.
2. Johnson, R. T. 2005. Prion diseases. *Lancet Neurol.* 4:635–642.
3. Naslavsky, N., H. Shmeeda, G. Friedlander, A. Yanai, A. H. Futerman, Y. Barenholz, and A. Taraboulos. 1999. Sphingolipid depletion increases formation of the scrapie prion protein in neuroblastoma cells infected with prions. *J. Biol. Chem.* 274:20763–20771.
4. Pinheiro, T. J. 2006. The role of rafts in the fibrillization and aggregation of prions. *Chem. Phys. Lipids*. 141:66–71.

5. Thellung, S., T. Florio, A. Corsaro, S. Arena, M. Merlino, M. Salmona, F. Tagliavini, O. Bugiani, G. Forloni, and G. Schettini. 2000. Intracellular mechanisms mediating the neuronal death and astrogliosis induced by the prion protein fragment 106-126. *Int. J. Dev. Neurosci.* 18:481–492.
6. Kourie, J. I. 2001. Mechanisms of prion-induced modifications in membrane transport properties: implications for signal transduction and neurotoxicity. *Chem. Biol. Interact.* 138:1–26.
7. Mironov, A., Jr., D. Latawiec, H. Wille, E. Bouzamondo-Bernstein, G. Legname, R. A. Williamson, D. Burton, S. J. DeArmond, S. B. Prusiner, and P. J. Peters. 2003. Cytosolic prion protein in neurons. *J. Neurosci.* 23:7183–7193.
8. Campana, V., D. Sarnataro, and C. Zurzolo. 2005. The highways and byways of prion protein trafficking. *Trends Cell Biol.* 15:102–111.
9. Forloni, G., N. Angeretti, R. Chiesa, E. Monzani, M. Salmona, O. Bugiani, and F. Tagliavini. 1993. Neurotoxicity of a prion protein fragment. *Nature.* 362:543–546.
10. Selvaggini, C., L. De Gioia, L. Cantu, E. Ghibaudi, L. Diomede, F. Passerini, G. Forloni, O. Bugiani, F. Tagliavini, and M. Salmona. 1993. Molecular characteristics of a protease-resistant, amyloidogenic and neurotoxic peptide homologous to residues 106–126 of the prion protein. *Biochem. Biophys. Res. Commun.* 194:1380–1386.
11. Florio, T., S. Thellung, C. Amico, M. Robello, M. Salmona, O. Bugiani, F. Tagliavini, G. Forloni, and G. Schettini. 1998. Prion protein fragment 106-126 induces apoptotic cell death and impairment of L-type voltage-sensitive calcium channel activity in the GH3 cell line. *J. Neurosci. Res.* 54:341–352.
12. Fioriti, L., E. Quaglio, T. Massignan, L. Colombo, R. S. Stewart, M. Salmona, D. A. Harris, G. Forloni, and R. Chiesa. 2005. The neurotoxicity of prion protein (PrP) peptide 106-126 is independent of the expression level of PrP and is not mediated by abnormal PrP species. *Mol. Cell. Neurosci.* 28:165–176.
13. Salmona, M., G. Forloni, L. Diomede, M. Algeri, L. De Gioia, N. Angeretti, G. Giaccone, F. Tagliavini, and O. Bugiani. 1997. A neurotoxic and gliotrophic fragment of the prion protein increases plasma membrane microviscosity. *Neurobiol. Dis.* 4:47–57.
14. De Gioia, L., C. Selvaggini, E. Ghibaudi, L. Diomede, O. Bugiani, G. Forloni, F. Tagliavini, and M. Salmona. 1994. Conformational polymorphism of the amyloidogenic and neurotoxic peptide homologous to residues 106-126 of the prion protein. *J. Biol. Chem.* 269:7859–7862.
15. Jobling, M. F., L. R. Stewart, A. R. White, C. McLean, A. Friedhuber, F. Maher, K. Beyreuther, C. L. Masters, C. J. Barrow, S. J. Collins, and R. Cappai. 1999. The hydrophobic core sequence modulates the neurotoxic and secondary structure properties of the prion peptide 106-126. *J. Neurochem.* 73:1557–1565.
16. Brown, D. R., J. Herms, and H. A. Kretzschmar. 1994. Mouse cortical cells lacking cellular PrP survive in culture with a neurotoxic PrP fragment. *Neuroreport.* 5:2057–2060.
17. Hope, J., M. S. Shearman, H. C. Baxter, A. Chong, S. M. Kelly, and N. C. Price. 1996. Cytotoxicity of prion protein peptide (PrP106-126) differs in mechanism from the cytotoxic activity of the Alzheimer's disease amyloid peptide, A β 25-35. *Neurodegeneration.* 5:1–11.
18. Pietri, M., A. Caprini, S. Mouillet-Richard, E. Pradines, M. Ermonval, J. Grassi, O. Kellermann, and B. Schneider. 2006. Overstimulation of PrPC signaling pathways by prion peptide 106-126 causes oxidative injury of bioaminergic neuronal cells. *J. Biol. Chem.* 281:28470–28479.
19. Lin, M. C., T. Mirzabekov, and B. L. Kagan. 1997. Channel formation by a neurotoxic prion protein fragment. *J. Biol. Chem.* 272:44–47.
20. Kourie, J. I., and A. Culverson. 2000. Prion peptide fragment PrP[106-126] forms distinct cation channel types. *J. Neurosci. Res.* 62:120–133.
21. Manunta, M., B. Kunz, E. Sandmeier, P. Christen, and H. Schindler. 2000. Reported channel formation by prion protein fragment 106-126 in planar lipid bilayers cannot be reproduced. *FEBS Lett.* 474:255–256.
22. Kunz, B., E. Sandmeier, and P. Christen. 1999. Neurotoxicity of prion peptide 106-126 not confirmed. *FEBS Lett.* 458:65–68.
23. Diomede, L., S. Sozzani, W. Luini, M. Algeri, L. De Gioia, R. Chiesa, P. M. Lievens, O. Bugiani, G. Forloni, F. Tagliavini, and M. Salmona. 1996. Activation effects of a prion protein fragment [PrP-(106-126)] on human leucocytes. *Biochem. J.* 320:563–570.
24. Ferreiro, E., R. Resende, R. Costa, C. R. Oliveira, and C. M. Pereira. 2006. An endoplasmic-reticulum-specific apoptotic pathway is involved in prion and amyloid-β peptides neurotoxicity. *Neurobiol. Dis.* 23:669–678.
25. Fioriti, L., N. Angeretti, L. Colombo, A. De Luigi, A. Colombo, C. Manzoni, M. Morbin, F. Tagliavini, M. Salmona, R. Chiesa, and G. Forloni. 2007. Neurotoxic and gliotrophic activity of a synthetic peptide homologous to Gerstmann-Straussler-Scheinker disease amyloid protein. *J. Neurosci.* 27:1576–1583.
26. LeVine 3rd, H. 1993. Thioflavine T interaction with synthetic Alzheimer's disease β-amyloid peptides: detection of amyloid aggregation in solution. *Protein Sci.* 2:404–410.
27. Klunk, W. E., R. F. Jacob, and R. P. Mason. 1999. Quantifying amyloid β-peptide (Aβ) aggregation using the Congo red-Aβ (CR-Aβ) spectrophotometric assay. *Anal. Biochem.* 266:66–76.
28. Sabate, R., and J. Estelrich. 2003. Pinacyanol as effective probe of fibrillar β-amyloid peptide: comparative study with Congo red. *Biopolymers.* 72:455–463.
29. Bertsch, M., A. L. Mayburd, and R. J. Kassner. 2003. The identification of hydrophobic sites on the surface of proteins using absorption difference spectroscopy of bromophenol blue. *Anal. Biochem.* 313: 187–195.
30. McParland, V. J., N. M. Kad, A. P. Kalverda, A. Brown, P. Kirwin-Jones, M. G. Hunter, M. Sunde, and S. E. Radford. 2000. Partially unfolded states of β (2)-microglobulin and amyloid formation in vitro. *Biochemistry.* 39:8735–8746.
31. Veiga, S., Y. Yuan, X. Li, N. C. Santos, G. Liu, and M. A. Castanho. 2006. Why are HIV-1 fusion inhibitors not effective against SARS-CoV? Biophysical evaluation of molecular interactions. *Biochim. Biophys. Acta.* 1760:55–61.
32. Ladokhin, A. S., S. Jayasinghe, and S. H. White. 2000. How to measure and analyze tryptophan fluorescence in membranes properly, and why bother? *Anal. Biochem.* 285:235–245.
33. Mayer, L. D., M. J. Hope, and P. R. Cullis. 1986. Vesicles of variable sizes produced by a rapid extrusion procedure. *Biochim. Biophys. Acta.* 858:161–168.
34. Cooper, M. A., A. Hansson, S. Lofas, and D. H. Williams. 2000. A vesicle capture sensor chip for kinetic analysis of interactions with membrane-bound receptors. *Anal. Biochem.* 277:196–205.
35. Keller, C. A., K. Glasmastar, V. P. Zhdanov, and B. Kasemo. 2000. Formation of supported membranes from vesicles. *Phys. Rev. Lett.* 84: 5443–5446.
36. Gaidukov, L., A. Fish, and A. Mor. 2003. Analysis of membrane-binding properties of dermaseptin analogues: relationships between binding and cytotoxicity. *Biochemistry.* 42:12866–12874.
37. Kamimori, H., K. Hall, D. J. Craik, and M. I. Aguilar. 2005. Studies on the membrane interactions of the cyclotides kalata B1 and kalata B6 on model membrane systems by surface plasmon resonance. *Anal. Biochem.* 337:149–153.
38. Mozsolits, H., and M. I. Aguilar. 2002. Surface plasmon resonance spectroscopy: an emerging tool for the study of peptide-membrane interactions. *Biopolymers.* 66:3–18.
39. Cooper, M. A. 2003. Label-free screening of bio-molecular interactions. *Anal. Bioanal. Chem.* 377:834–842.
40. Henriques, S. T., and M. A. Castanho. 2004. Consequences of nonlytic membrane perturbation to the translocation of the cell penetrating peptide pep-1 in lipidic vesicles. *Biochemistry.* 43:9716–9724.
41. Caputo, G. A., and E. London. 2003. Using a novel dual fluorescence quenching assay for measurement of tryptophan depth within lipid bilayers to determine hydrophobic α-helix locations within membranes. *Biochemistry.* 42:3265–3274.
42. Gross, E., R. S. Bedlack Jr., and L. M. Loew. 1994. Dual-wavelength ratiometric fluorescence measurement of the membrane dipole potential. *Biophys. J.* 67:208–216.

43. Cladera, J., and P. O'Shea. 1998. Intramembrane molecular dipoles affect the membrane insertion and folding of a model amphiphilic peptide. *Biophys. J.* 74:2434–2442.

44. Tagliavini, F., F. Prelli, L. Verga, G. Giaccone, R. Sarma, P. Gorevic, B. Ghetti, F. Passerini, E. Ghibaudi, G. Forloni, et al. 1993. Synthetic peptides homologous to prion protein residues 106-147 form amyloid-like fibrils in vitro. *Proc. Natl. Acad. Sci. USA.* 90:9678–9682.

45. Groenning, M., L. Olsen, M. van de Weert, J. M. Flink, S. Frokjaer, and F. S. Jorgensen. 2007. Study on the binding of Thioflavin T to β-sheet-rich and non-β-sheet cavities. *J. Struct. Biol.* 158:358–369.

46. Inouye, H., and D. A. Kirschner. 2000. A β fibrillogenesis: kinetic parameters for fibril formation from Congo red binding. *J. Struct. Biol.* 130:123–129.

47. Inouye, H., and D. A. Kirschner. 2005. Alzheimer's β-amyloid: insights into fibril formation and structure from Congo red binding. *Subcell. Biochem.* 38:203–224.

48. Gennis, R. B. 1989. Biomembranes Molecular Structure and Function. Springer-Verlag, New York.

49. Zhao, H., E. K. Tuominen, and P. K. Kinnunen. 2004. Formation of amyloid fibers triggered by phosphatidylserine-containing membranes. *Biochemistry.* 43:10302–10307.

50. Taraboulos, A., M. Scott, A. Semenov, D. Avrahami, L. Laszlo, and S. B. Prusiner. 1995. Cholesterol depletion and modification of COOH-terminal targeting sequence of the prion protein inhibit formation of the scrapie isoform. *J. Cell Biol.* 129:121–132.

51. Bate, C., M. Salmona, L. Diomede, and A. Williams. 2004. Squalestatin cures prion-infected neurons and protects against prion neurotoxicity. *J. Biol. Chem.* 279:14983–14990.

52. Reyes Mateo, C., A. Ulises Acuna, and J. C. Brochon. 1995. Liquid-crystalline phases of cholesterol/lipid bilayers as revealed by the fluorescence of trans-parinaric acid. *Biophys. J.* 68:978–987.

53. Choo-Smith, L. P., W. Garzon-Rodriguez, C. G. Glabe, and W. K. Surewicz. 1997. Acceleration of amyloid fibril formation by specific binding of Aβ-(1-40) peptide to ganglioside-containing membrane vesicles. *J. Biol. Chem.* 272:22987–22990.

54. Choo-Smith, L. P., and W. K. Surewicz. 1997. The interaction between Alzheimer amyloid β (1-40) peptide and ganglioside GM1-containing membranes. *FEBS Lett.* 402:95–98.

55. Kakio, A., S. Nishimoto, K. Yanagisawa, Y. Kozutsumi, and K. Matsuzaki. 2002. Interactions of amyloid β-protein with various gangliosides in raft-like membranes: importance of GM1 ganglioside-bound form as an endogenous seed for Alzheimer amyloid. *Biochemistry.* 41:7385–7390.

56. Chi, E. Y., S. L. Frey, and K. Y. Lee. 2007. Ganglioside G(M1)-mediated amyloid-β fibrillogenesis and membrane disruption. *Biochemistry.* 46:1913–1924.

57. Shi, J., T. Yang, S. Kataoka, Y. Zhang, A. J. Diaz, and P. S. Cremer. 2007. GM1 clustering inhibits cholera toxin binding in supported phospholipid membranes. *J. Am. Chem. Soc.* 129:5954–5961.

58. Tillack, T. W., M. Wong, M. Allietta, and T. E. Thompson. 1982. Organization of the glycosphingolipid asialo-GM1 in phosphatidylcholine bilayers. *Biochim. Biophys. Acta.* 691:261–273.

59. Magzoub, M., A. Pramanik, and A. Graslund. 2005. Modeling the endosomal escape of cell-penetrating peptides: transmembrane pH gradient driven translocation across phospholipid bilayers. *Biochemistry.* 44:14890–14897.

60. Whittingham, J. L., D. J. Scott, K. Chance, A. Wilson, J. Finch, J. Brange, and G. Guy Dodson. 2002. Insulin at pH 2: structural analysis of the conditions promoting insulin fibre formation. *J. Mol. Biol.* 318:479–490.

61. Seelig, J. 2004. Thermodynamics of lipid-peptide interactions. *Biochim. Biophys. Acta.* 1666:40–50.

62. White, S. H., and W. C. Wimley. 1998. Hydrophobic interactions of peptides with membrane interfaces. *Biochim. Biophys. Acta.* 1376:339–352.

63. Magzoub, M., and A. Graslund. 2004. Cell-penetrating peptides: [corrected] from inception to application. *Q. Rev. Biophys.* 37:147–195.

64. Henriques, S. T., M. N. Melo, and M. A. Castanho. 2006. Cell-penetrating peptides and antimicrobial peptides: how different are they? *Biochem. J.* 399:1–7.

65. Magzoub, M., S. Sandgren, P. Lundberg, K. Oglecka, J. Lilja, A. Wittrup, L. E. Goran Eriksson, U. Langel, M. Belting, and A. Graslund. 2006. N-terminal peptides from unprocessed prion proteins enter cells by macropinocytosis. *Biochem. Biophys. Res. Commun.* 348:379–385.

66. Kazlauskaite, J., N. Sanghera, I. Sylvester, C. Venien-Bryan, and T. J. Pinheiro. 2003. Structural changes of the prion protein in lipid membranes leading to aggregation and fibrillization. *Biochemistry.* 42:3295–3304.

67. Sanghera, N., and T. J. Pinheiro. 2002. Binding of prion protein to lipid membranes and implications for prion conversion. *J. Mol. Biol.* 315: 1241–1256.